The ancestral Rocky Mountain orogeny and evolution of the Permian Basin

Kurt Rudolph

2023, pp. 68-75. https://doi.org/10.56577/FFC-73.68
Supplemental data: https://nmgs.nmt.edu/repository/index.cfml?rid=2023001

in:

Evaporite Karst of the Lower Pecos Region, Land, Lewis; Bou Jaoude, Issam; Hutchinson, Peter; Zeigler, Kate; Jakle, Anne; Van Der Werff, Brittney, New Mexico Geological Society 73 rd Annual Fall Field Conference Guidebook, 152 p. https://doi.org/10.56577/FFC-73

This page is intentionally left blank to maintain order of facing pages.

New Mexico Geological Society Guidebook, 73rd Fall Field Conference, 2023, p. 68–75, https://doi.org/10.56577/FFC-73.68

THE ANCESTRAL ROCKY MOUNTAIN OROGENY AND EVOLUTION OF THE PERMIAN BASIN

KURT RUDOLPH

Rice University/University of Houston, 202 Willard St., Houston, TX 77006; kwrudolph@comcast.net

Abstract—The Permian Basin is a mosaic of basins and platforms that formed in the late Paleozoic associated with compressional deformation of the Ancestral Rocky Mountains or "ARM" Orogeny. This event partitions the predecessor broad/shallow early Paleozoic Tobosa Basin. The timing of late Paleozoic basin formation is evaluated using calibrated basin models to analyze total subsidence. Two subsidence phases are interpreted—an initial period of Late Pennsylvanian to early Permian (~305–285 Ma) rapid subsidence of the basins, contrasted with very slow subsidence or uplift of the platforms. The first phase of subsidence is coeval with the flexural foreland basin subsidence in the Val Verde Basin, which is related to the thin-skinned Marathon Orogeny. While this may indicate a kinematic linkage, structural styles are very different. The most important tectonic unconformity occurs near the end of this phase, in the early Permian (Wolfcampian). The lower Wolfcampian Unconformity erodes deeply on the Central Basin Platform, Diablo Platform, and Pedernal Uplift. The interval below the unconformity is commonly significantly deformed, while the interval above is only gently folded. The second phase of subsidence is characterized by rapid and relatively uniform subsidence of the entire area, both platforms and basins, from Leonardian to Ochoan (~285–250 Ma) time. The drivers of the second phase of subsidence are less clear. Also, the timing of the onset in the Permian Basin is younger than other portions of the ARM and Ouachita orogenic belts; this may imply later collisional tectonics in the southwestern part of the system.

INTRODUCTION AND GEOLOGIC SETTING

The Permian Basin of west Texas and southeastern New Mexico is a complex, partitioned late Paleozoic province composed of discrete subbasins and uplifts (Fig. 1; Ruppel, 2019). It is considered a component of a family of intracratonic basins and associated uplifts termed the "Ancestral Rocky Mountains," or "ARM" (Kluth and Coney, 1981). These stretch from Kansas/Oklahoma in the east to Nevada in the west (Fig. 1). Characterized by discrete basement-involved uplifts, the basins have a variety of orientations and sedimentary fills. ARM structural deformation is dominantly contractional, with secondary transpressional elements (Sweet et al., 2021).

To the south of the ARM Permian Basin lies the coeval Marathon Orogenic Belt and associated Val Verde and Marathon foreland basins. This is a southwestern extension of the late Paleozoic Ouachita thin-skinned system that is a product of the collision of Laurentia and Gondwana (Dickinson and Lawton, 2003).

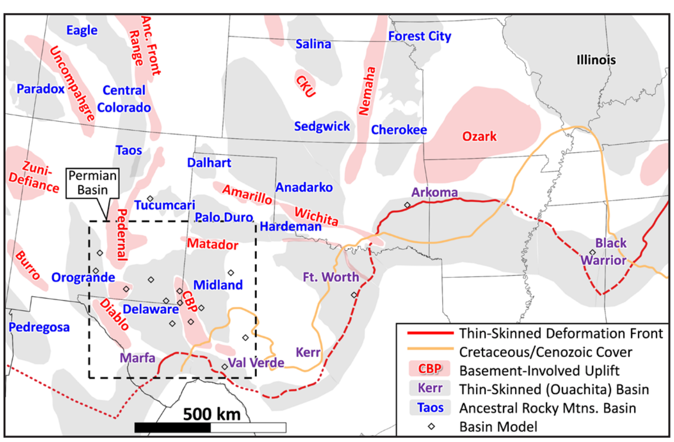

FIGURE 1. Regional map of late Paleozoic tectonic features and basin models referred to in this study. Basins are in grey and are from USGS ArcGIS coverages. ARM basins are labelled in blue and forelands in purple. Some ARM basins (e.g., Oquirrh) lie west of map area. CBP and CKU refer to Central Basin Platform and Central Kansas Uplift, respectively. Dashed box is area of Figure 2 and is the study area of this paper.

Prior to the development of the Permian Basin in the late Paleozoic, the area was on a long-lived passive margin, with deep-water and oceanic crust to the south (Ruppel, 2019). This low-relief depocenter, the Tobosa Basin, is filled by ramp carbonates and siliciclastics of late Cambrian to Mississippian age.

An area of discussion is the relationship between the interior, thick-skinned deformation of the ARM basins (e.g., Permian Basin) to the thin-skinned Ouachita Orogeny (e.g., Marathon Fold Belt) to the south (Dickinson and Lawton, 2003; Leary et al., 2017; Kluth and Coney, 1981). A useful partial analogy is the temporally overlapping Laramide (thick-skinned) and Sevier (thin-skinned) orogenies of the Jurassic-Eocene Cordillera of the U.S. Western Interior (Yonkee and Weill, 2015). In this case, there is consensus that the plate-scale controls change, but have continuity, with an evolution of structural style related to a change in subduction style (Dickinson et al., 1988). Leary et al. (2017) emphasized the three-sided nature of the orogeny, which can be viewed as a complementary geodynamic explanation for the widespread deformation of the Laurentian interior. In the analysis of the Permian Basin, an evaluation of timing is used to evaluate the potential geodynamic/kinematic linkage of the Ouachita and ARM systems.

As the most prolific hydrocarbon province in North America, with a rich database of subsurface and outcrop data, the Permian Basin has been extensively studied over the decades. Still, the complex tectono-stratigraphic history invites further analysis. This study evaluates the basin response to late Paleozoic orogenesis by subsidence analysis (calibrated basin models) of both basins and uplifts. It is placed within the context of a larger-scale screening analysis of Paleozoic subsidence and flexural effects of North America (Fig. 1) that utilizes the same approach.

On a more detailed level, paleogeographic elements include the Delaware and Midland basins, Central Basin and Diablo platforms, the Pedernal Uplift, and Northwest and Eastern shelves (Fig. 2). The western portion of the Permian Basin has experienced extension, with associated foot-wall uplift, during Neogene Basin and Range deformation. This has exposed much of the late Paleozoic section in the Guadalupe, Delaware, Sierra Diablo, Hueco, and Sacramento Mountains (Fig. 2). Observations from these exposures provide additional insights into the structural and stratigraphic history.

METHODS

Introduction

This study leverages the vast published literature and public domain well data available through the New Mexico and Texas state websites. (Not all sources for minor input are cited herein.) The intent is to reevaluate the subsidence history utilizing established well and outcrop-based chronostratigraphy from the literature, augmented by extending this stratigraphy into uncorrelated wells. Of special interest was the evaluation of the relationship between uplifts and basins. The geologic timescale of Gradstein et al. (2020), as implemented in their program Time Scale Creator 8.0, was employed.

Basin Models

The Schlumberger application Petromod© was used to construct 1D basin models in the Permian Basin. The primary inputs are the depths, geologic age, and lithology of the stratigraphic horizons. At each surface, paleobathymetry/paleoelevation, basal heat flow, and paleo-surface temperature must also be defined. The program "backstrips" (decompacts) the section, layer by layer, to the oldest horizon. The effect of both sediment and water load are included in the calculations. Erosion of sedimentary section can also be specified, whether it is associated with ancient unconformities or Neogene exhumation. Reconstructing the missing section (age, thickness, and lithology) can be a challenge, relying either on projection from areas where the missing section is preserved or paleotemperature indicators at the location.

Three families of products are generated: depth plots, time plots, and burial history plots. The parameters of temperature, vitrinite reflectance, porosity, pressure, and thermal conductivity can be displayed in any of these domains. In this study, we have only illustrated the burial history, as exported and redisplayed in Excel©. Basin model inputs are included in Supplement 1.

There are two complementary objectives of basin models. First, to quantitatively evaluate the subsidence history. Second, to analyze and predict key parameters over geologic time and depth, especially petroleum source rock maturation. The latter application requires a good understanding of the heat flow history. To test and refine the assumptions on heat flow and burial history, calibrations of model outputs against observed present day temperature and vitrinite reflectance versus depth are important, if questions of temperature and/or exhumation history are of interest (Hantschel and Kauerauf, 2009).

As the objective of this analysis is to comprehend the

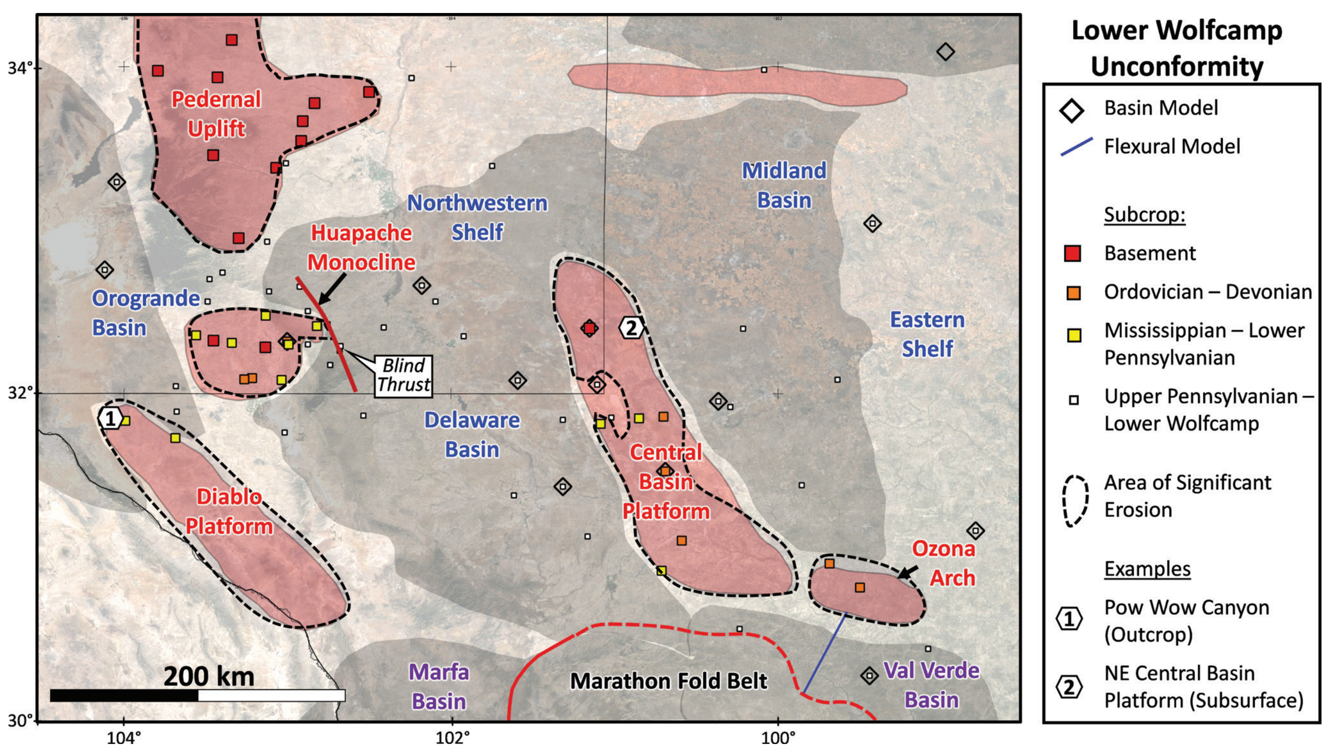

FIGURE 2. Map of Permian Basin with paleogeographic and tectonic elements for the late Paleozoic. Refer to Figure 1 for additional legend references and larger context. The dashed-line polygons are interpreted areas of significant erosion associated with the Lower Wolfcampian Unconformity from well penetrations, plus the outcrop ("1") described in Figure 4. Mountain outcrops are: G-Guadalupe, De-Delaware, Di-Diablo, H-Hueco, and S-Sacramento. See text for further explanation.

subsidence history, heat flow is usually not as important, and only a few calibrations have been completed. However, in cases where a significant amount of the section of interest has been removed by recent erosion, calibration becomes critical. In this study, basal heat flow has been interpreted as constant from Paleozoic to present, and the regional U.S. heat flow map developed by SMU served as an initial estimate (Blackwell et al., 2011).

As indicated by clinoforms observed in outcrop, on seismic data, and on well log cross sections, the late Pennsylvanian to Permian basins were deep, with fairly to very steep margins (Ruppel, 2019). Therefore, accurate characterization of paleobathymetry is important to develop reliable subsidence histories. In this analysis, a wide variety of cross sections were employed, such as the west Texas Geological Society suite (e.g., Matchus and Jones, 1984). A key touchstone is the regional outcrop and well-based cross section from the Northwest Shelf to Delaware Basin of Kerans and Kempter (2002). This is extremely well-documented and also leverages the ~1.2 km high exposures of the Western Escarpment of the Guadalupe Mountains. Inputs to the basin models are documented in Supplement 1.

Flexural Modeling

A flexural model for the Val Verde Basin was constructed and is based on the cross section of upper Pennsylvanian to lower Wolfcampian strata documented in Hamlin (2009). The primary inputs are thickness control points with their position relative to the front of the load. Also specified are the permitted stratigraphic uncertainty/error ranges; acceptable ranges on tectonic load density, front load position, load width and height; and taper direction and maximum slope angle, range of effective elastic thickness (or "EET"), and range of load and sediment fill densities. The software used is the MATLAB© code, "FlexMC" (Saylor et al., 2017); the algorithm uses the equations set out by Wangen (2010). Trials that meet the uncertainty criteria are tabulated and reported (means and standard deviations). This model also assumes a northwards taper to the load, consistent with structural cross sections of the Marathon Fold Belt (Hickman et al., 2009). Thus, few assumptions are made on the flexural controls, and the results are observationally driven. The most important parameters estimated from the modeling are load height, topographic height, load width, slope, and effective elastic thickness. The model shown assumes an infinite plate; results for a broken plate were also tested and found to be similar.

To clarify, effective elastic thickness is a measure of the flexural strength of the coupled lithosphere. High EET yields a broad, but shallow foreland, whereas low EET yields a narrow but deep foreland for the equivalent load (Beaumont, 1981).

RESULTS AND DISCUSSION

Basin Modeling

Of the thirteen basin models in the study area, seven have a complete Permian section preserved. Five sites have had some Ochoan or upper Guadalupian to Ochoan strata restored, all estimated at less than 300 m. But the Val Verde foreland basin has had significant exhumation of the thick foredeep, presumably due to flexural rebound as the fold belt was eroded. In wells, the upper Wolfcampian is the youngest Paleozoic section preserved and subcrops beneath about 300 m of Cretaceous limestone cover. Projections from the north indicate a thick section of upper Wolfcampian to Ochoan strata was likely present (Fig. 6). Moreover, vitrinite reflectance (VR) data in the area indicate significant paleoburial of the upper part of the preserved Paleozoic section, with a VR ≈ 0.7 (data of Pawlewicz et al., 2005). In this instance, a detailed calibration was completed; an estimated restored section of about 1600 m is necessary to explain the thermal maturity. An increase of ~0.7%Ro VR and ~30°C maximum temperature at the Woodford Shale level (~3150 m subsea depth) is implied by including additional Permian burial at this site (Supplement 4).

The eleven basin models from the Permian Basin and two from the Orogrande Basin (not shown) have three contemporaneous subsidence events, with important variability in magnitude (Fig. 3). There is an initial late Cambrian–Ordovician phase of moderate subsidence that has been interpreted as related to modest extension and passive margin sag on the southern margin of Laurentia (Phase 0, Fig. 3; Ewing, 2019).

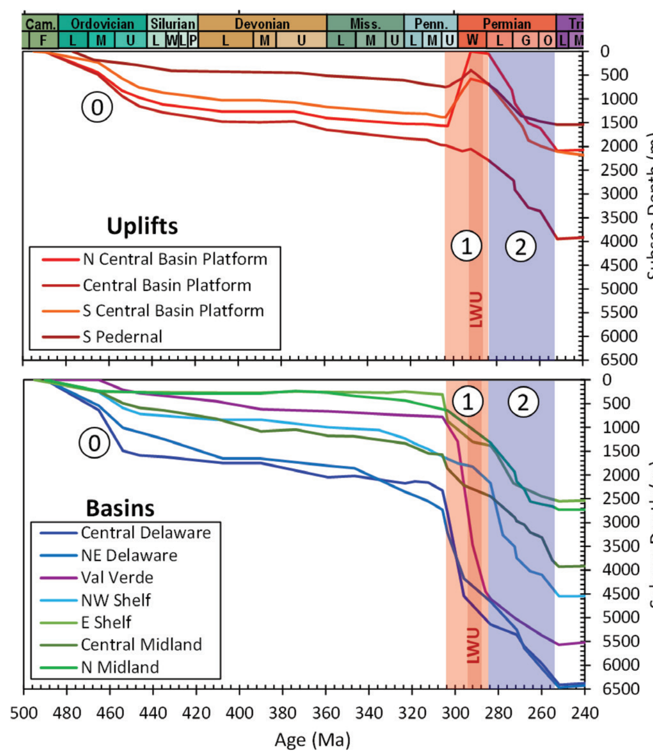

FIGURE 3. Total subsidence from selected sites within the Permian Basin, with late Paleozoic uplifts at top and basins at bottom. Late Cambrian to Ordovician subsidence (0) is attributed to extension and sag on a passive margin. The initial late Paleozoic phase (1) from ~305–285 Ma is characterized by highly variable subsidence and uplift, which differentiated the basin. A second phase (2) has more uniform subsidence, with both uplifts and basins foundering at about the same rate. "LWU" indicates the approximate position of the Lower Wolfcampian Unconformity. Locations of models are on Figure 2. Basin models were built using PetroMod© basin modeling software.

This is a widespread motif throughout Laurentia and has been attributed to the breakup of a portion of the Pannotia or Rodinia supercontinent from 625–550 Ma in the Tobosa Basin area (Bond et al., 1984; Ewing, 2019).

Commencing at about 305 Ma (top Desmoinesian Stage, or top Strawn Formation equivalent), there is a marked increase in total subsidence in the Midland, Delaware, and Val Verde basins, as well as the Northwest Shelf and Eastern Shelf (Phase 1, Fig. 3). A similar inflection is observed in the Orogrande Basin to the west (Supplement 3). In contrast, uplifts such as the Central Basin Platform and Pedernal Uplift were subsiding slowly or being uplifted at this time. This variable subsidence and uplift partitioned the basin and created the familiar paleogeography seen in Figure 2. Moreover, this created a dramatic differentiation of lithofacies, with uplifts and basin margins dominated by highstand carbonates, and basin deep sediments comprised mostly of lowstand submarine fan sandstones and thin basinal carbonates (first described by Silver and Todd, 1969).

There is some ambiguity in the onset of subsidence, if thicknesses in the Marathon Fold Belt are considered. While uniformly thin in the preserved foredeep, a thick, deformed interval of upper Mississippian to lower Pennsylvanian turbidites (Tesnus Formation) is described from outcrop and wells (McBride, 1978). This interval is interpreted as thickening to the south (Chapman and McCarthy, 2013), reaching 2–3 km in thickness. Several hypotheses are entertained here. First, the Tesnus could be an indicator of the onset of the Gondwana collision/Marathon Orogeny. Second, this could be a precursor Andean-style margin (subducting ocean beneath Laurentia). Third, the Tesnus represents the filling of very deep-water, passive margin accommodation, as evidenced by the underlying Ordovician Maravillas Chert and Silurian to lower Mississippian Caballos Novaculite.

The mechanism for this first phase of subsidence in the Permian Basin is uncertain (Ewing, 1993, 2019; Ewing and Christensen, 2016; Zhang et al., 2021). In part, Ewing invokes an elevator basin analogy for ARM basins, which includes strike-slip faulting as a mechanism. Compared to other ARM basins, both the Anadarko and Paradox appear purely flexural in origin (Garner and Turncotte, 1984; Barbeau, 2003). This result has been confirmed by independent modeling by the author (Rudolph, 2021; Eichler and Rudolph, 2023).

I conjecture that flexural loading of the uplifts on the margins of the basins may be a contributor, especially for the Delaware. Significant structural relief exists between the Delaware Basin and Central Basin Platform, Diablo Platform, Pedernal Uplift, and Huapache Uplift (Fig. 2). For example, at basement level, the structural relief between the Central Basin Platform and Delaware and Midland basins is about 4.2 and 1.6 km over distances of less than 5 km, respectively (map from Loucks and Kerans, 2019). This is in addition to the load associated with the Marathon Orogenic Belt, which likely influenced subsidence in the southernmost Delaware Basin. However, in contrast to the Anadarko and Paradox examples, this is a complex 3D problem—simple 2D profiles are unlikely to illustrate much of a flexural wedge because of the interference of the other loads. With only the Central Basin Platform as a potential load, a flexural origin is more difficult to postulate for the Midland Basin, although it may have contributed.

At approximately 285 Ma (near top of Wolfcampian), the subsidence mode changes, with both basins and uplifts subsiding at about the same rapid rate (Phase 2, Fig. 3). This continues until the end of the Permian (ca. 252 Ma). Therefore, this is a long-wavelength subsidence event, creating fairly uniform accommodation space over a very large area. Based on this geometry, a flexural origin can be ruled out. Events of this sort are often interpreted as dynamic subsidence, related to deep crustal and mantle processes (Liu et al., 2014). If ARM deformation is related to flat-slab subduction (Ye et al., 1996), as interpreted for the Laramide Orogeny, then some form of interaction between the overlying and underlying plate might have merit as an explanation (Ye et al., 1996); however, this geodynamic explanation remains speculative (Kluth, 1998). Soreghan et al. (2012) interpreted the long-wavelength subsidence phase at the end of ARM deformation as driven by the effects of a high-density mafic crustal load, emplaced during Cambrian rifting.

An important result is that the subsidence of the Val Verde foreland basin is synchronous with the ARM basins to the north (Fig. 3). So, while structural style and potentially the mechanism of subsidence is different, a kinematic linkage can be inferred by timing.

Lower Wolfcampian Unconformity

Punctuating late Paleozoic subsidence is a regional tectonic unconformity, developed on structural highs (Fig. 2; Supplement 2; Ewing, 2019). It occurs in the lower Wolfcampian, near the end of Phase 1 subsidence (Fig. 3). This angular unconformity is recognized from outcrop exposures in the Hueco Mountains (Fig. 4) and Sacramento Mountains (Spangler, 2021). In outcrop, the section resting above the unconformity is usually quite conglomeratic, containing both siliciclastic and carbonate cobbles. Cobbles are clast-supported, indicating water-lain deposition, and likely represent alluvial fan deposits on and flanking the uplifts (Fig. 4). This is also widely recognized on subsurface data, where the unconformity separates complexly folded (below) from gently deformed (above) strata (Fig. 5). As such, it marks the transition from Phase 1 to Phase 2 subsidence. Based on well and seismic control, the unconformity erodes as deep as basement, inferring up to 1.5 km of exhumation, based on the thickness of the restored section below the surface (Fig. 3). Structural growth strata are locally recognized in outcrop within the Sacramento Mountains in the upper Virgilian to lower Wolfcampian Bursum Formation (Spangler, 2021). But, usually, most of the structural deformation is fault propagation folds with parallel beds that are truncated at the surface, with potential growth strata removed by erosion.

In the basins, the upper Pennsylvanian to Wolfcampian section is conformable, although the Wolfcampian Detrital Play (Dutton et al., 2004) may be related to erosion of the adjacent uplifts. To better understand the distribution of this angular unconformity, an analysis of the subcrop relationships from well

FIGURE 4. Angular unconformity on the Diablo Platform (Pow Wow Canyon, Hueco Mountains). In this locale, Wolfcampian Pow Wow Conglomerate lies on Atokan-Morrowan cyclic carbonates and clastics of the Magdalena Formation. Here, the lacuna associated with the unconformity surface is about 20 million years. Inset: outcrop photo of the Pow Wow Conglomerate. See Figure 2 for location.

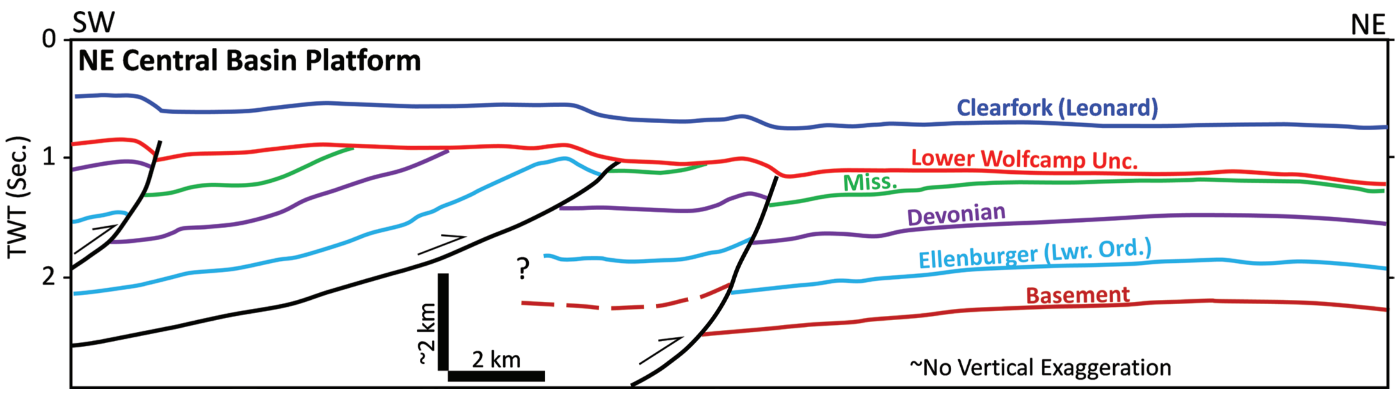

FIGURE 5. Interpreted structural cross section from northeast Central Basin Platform, based on seismic line, adapted from Ye et al. (1996). Contractional fault propagation folds are truncated by the lower Wolfcampian unconformity. The overlying Permian section is gently folded, with much less structural relief. TWT is two-way time, and the vertical scale in km is approximate (a constant velocity of 5 km/sec was used to convert to depth). See Figure 2 for location.

and outcrop data was conducted (Fig. 2). Most of the control points are from correlated well logs, but publications were sourced as well (King and Harder, 1985; Meyer, 1966). Where upper Pennsylvanian to lower Wolfcampian strata were interpreted below the unconformity, no significant erosion (<100 m) is interpreted.

Four areas of significant erosion were documented—Central Basin Platform, northern Pedernal Uplift, Diablo Platform, and a southern extension of the Pedernal Uplift that is interpreted to be associated with the Huapache Monocline (Fig. 2). The general outline on the Central Basin Platform is guided by the Ellenburger depth structure map (Fairhurst et al., 2012), with low areas on the uplift expected to be more conformable.

At the surface, the Huapache Monocline is a gentle fold of exposed Guadalupian strata (San Andres and Grayburg formations), dipping to ESE (Black, 1975). The monocline axis is oriented NNW-SSE and forms the western margin of the geomorphologic province called the Seven Rivers Embayment (Black, 1975; Price et al., 2022). The lower Wolfcampian Unconformity erodes as deeply as basement to the west of the monocline. Additionally, a well (30-015-00014) drilled on the forelimb penetrates a thick repeat section of Mississippian to Ordovician, indicating a major thrust fault at depth. This area seems to be a good analogy to the Central Basin Platform structural geometry (Fig. 5), with thrusted and folded pre-Wolfcampian strata below and subtle drape folding above.

As illustrated in Figure 5, the subcropping pattern below the lower Wolfcampian Unconformity is even more complicated than depicted on Figure 2. This is because the wavelength of the contractional folding is likely much smaller than can be defined with the limited control points.

Flexural Modeling

The Val Verde Basin is a thick wedge of upper Pennsylvanian to Wolfcampian deep-water shales and sandy turbidites that thin to the north (Fig. 6). As described in the methods section, the proximal foredeep has been significantly exhumed. But calibrated basin modeling and projection of thickness trends allows restoration of the missing Leonardian to Ochoan succession (1600 m at the basin model location). Note that the upper Pennsylvanian to middle Wolfcampian interval (below

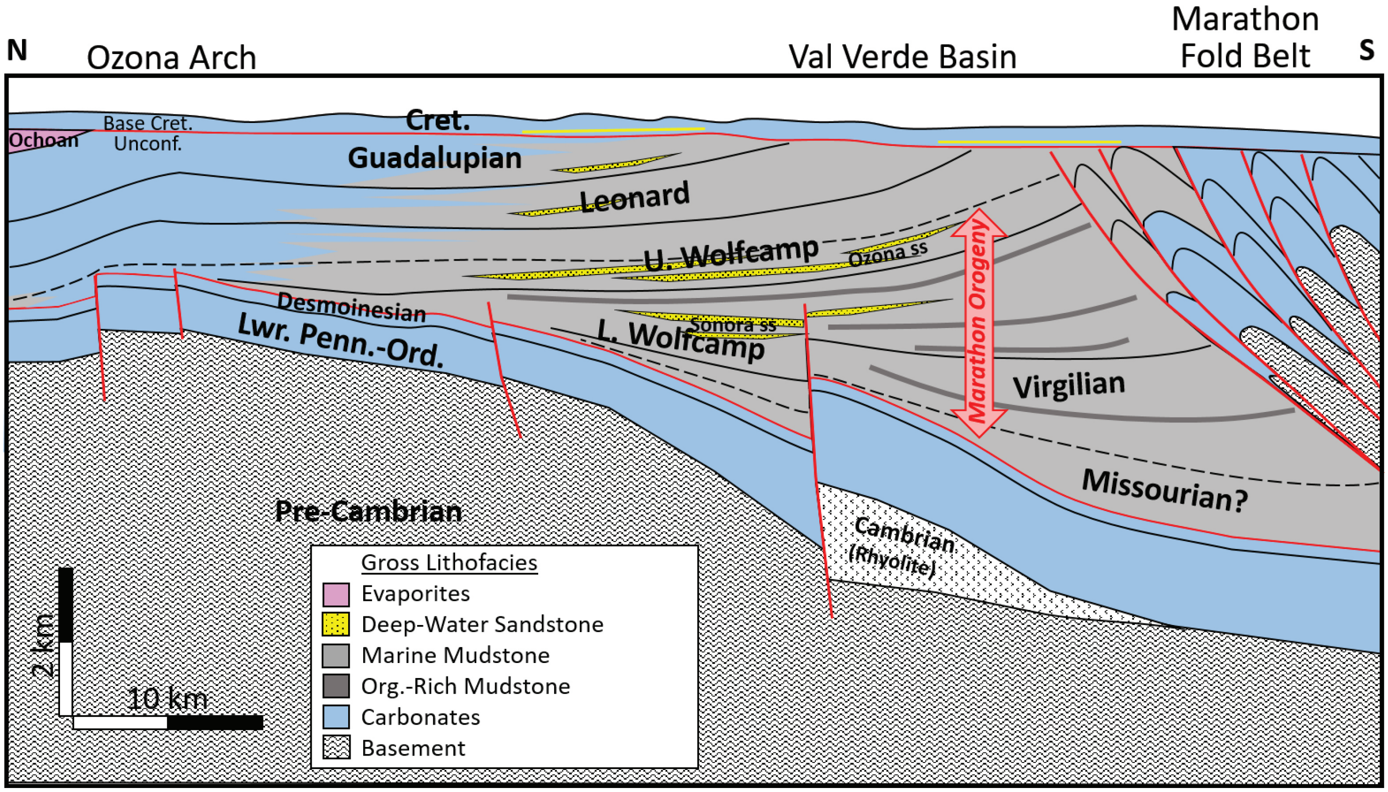

FIGURE 6. Semi-schematic cross section of Marathon Fold Belt and Val Verde Basin. Flexurally thickened wedge of deep-water foreland deposits are of Missourian to Wolfcampian age. Location is approximately the same as the flexural model and is shown on Figure 2. Based, in part, on Hamlin (2009) and Ewing (2019).

the dashed line on Fig. 6) has a strong wedge geometry, thinning to nearly zero onto the Ozona Arch. But above the dashed line (upper Wolfcampian to Guadalupian), the interval is more uniform in thickness and has a thick interval over the arch. This is consistent with the observations made for the Permian Basin as a whole.

The Val Verde Basin flexural model indicates that the basin geometry of the upper Pennsylvanian to middle Wolfcampian is consistent with a flexural origin, with loading associated with the Marathon Orogeny to the southwest. The wavelength of the flexure is quite small, about 100 km from load front to forebulge apex (Fig. 7). The position of the modeled forebulge is coincident with the Ozona Arch, which is an east-west oriented extension of the Central Basin Platform (Fig. 2). It has been postulated that the arch is a Marathon-related forebulge (Ewing, 2019). The lower Wolfcampian Unconformity erodes at least as deep as Ellenburger in some places on the arch, inferring the erosion of about 800–1100 m of section (Fig. 2). The modeled forebulge aggregates about that much relief over the modeled interval of Virgilian to middle Wolfcampian. However, the width of the Ozona Arch (~50 km) appears narrower than the modeled extent of the forebulge (~100 km). While a forebulge origin is a reasonable hypothesis, it is also possible that the arch (and southern terminus of the Central Basin Platform) are hybrid features with both ARM and forebulge characteristics.

Finally, the EET estimate from modeling yielded a mean of only 12 km, as would be expected for such a narrow basin. This is indicative of a very weak coupled lithosphere. Modern estimates of EET from seismic tomography yield an estimate of 10–25 km for this area (Tesauro et al., 2015), generally consistent with the Paleozoic modeling result.

Regional Subsidence Patterns

Placing the Permian Basin in a larger context facilitates an understanding of possible genetic linkages. Leveraging other basin models built (Figs. 1, 8), we can make several observations. The greater Permian Basin experienced a relatively late onset of rapid subsidence, compared to the greater Ouachita

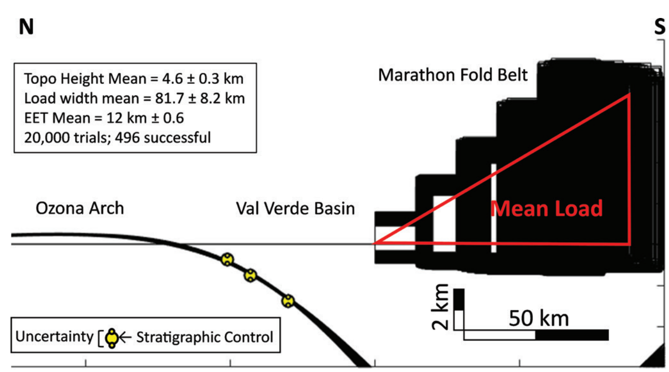

FIGURE 7. Flexural model, tied to stratigraphic control points, for the Val Verde Basin. Location is shown on Figures 1 and 2. This uses an inverse Monte Carlo modeling code that iteratively tests different load and flexural rigidity estimates to observations (Saylor et al., 2017). The close fit of the model results to the stratigraphic control points is consistent with the hypothesis that the Ozona Arch is a flexural bulge.

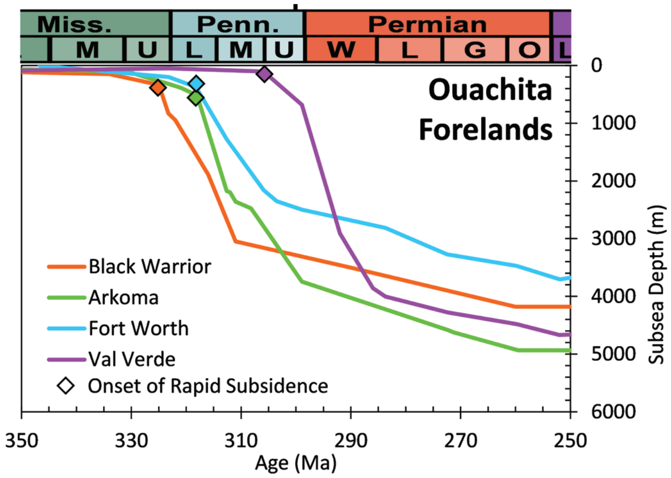

FIGURE 8. Basin models for foreland basins along the southern margin of Laurentia in the late Paleozoic subsidence. The onset of rapid subsidence, shown with the colored triangles, is about 20 million years younger in the northeast compared to the southwest, perhaps inferring a "scissor-closure" of Laurentia and Gondwana.

system. Specifically, the onset of rapid Val Verde subsidence begins later than in the Fort Worth and Arkoma basins, and much later than the Black Warrior Basin (Fig. 8). The onset of flexural subsidence becomes younger along this margin and has been interpreted as the east-west progressive suturing of Laurentian and Gondwana in the late Paleozoic (Ingersoll et al., 1995; Dickinson and Lawton, 2003). It has been interpreted as a progressive suturing of Laurentian and Gondwana associated with the assembly of Pangea in the late Paleozoic. The strongly diachronous nature is implied by subsidence analysis, indicating about 20 million years younger initiation from east to west (Fig. 8).

Additionally, the Permian Basin, and associated Orogrande and Tucumcari basins (Fig. 1, Supplement 3), are all relatively young when compared to other ARM basins (Sweet et al., 2021). The first phase of Permian Basin subsidence supports a kinematic linkage with the Marathon Fold Belt based on synchroneity. The second phase involves a change in the dominant style of subsidence, with the driving forces unclear. Moreover, this second phase is critical in making the Permian Basin a world class petroleum system, by pushing source rocks into the generative window and facilitating the deposition of important carbonate hydrocarbon reservoirs on the platforms such as the Clearfork, San Andres, and Grayburg formations.

CONCLUSIONS

Subsidence in the Permian Basin is comprised of two phases. First, the late Pennsylvanian to Wolfcampian phase is characterized by significant contractional deformation, differential subsidence of basins and uplift of platforms, and marked by a significant angular unconformity in the Wolfcampian. The second phase of subsidence is characterized by only mild deformation and subsidence of a broad area that includes both uplifts and basins. The first phase of Permian Basin subsidence history is synchronous with the Val Verde foreland basin. The Val Verde Basin is flexural in origin, and the Ozona Arch potentially represents a forebulge, at least in part.

The narrowness of the foredeep indicates a weak coupled lithosphere, consistent with modern estimates of EET. The second phase of Permian Basin subsidence appears to post-date the Marathon Orogeny and does not have a strong flexural subsidence influence. The Permian Basin has the latest onset of Ouachita/ARM subsidence, relative to other Ouachita and ARM basins. This spatial-temporal pattern of basin development is consistent with a model of east-west progressive closure along the southern Laurentian-Gondwanan margin. Furthermore, this model invokes this closure as the driver of ARM basin subsidence, at least for basins proximal to the collisional margin such as the Permian Basin.

ACKNOWLEDGMENTS

This paper benefitted from an early review by Kevin Biddle (Rice University) and later reviews by Jerry Kendall (UNM) and Tyson Smith (USGS).

REFERENCES

Barbeau, D.L., 2003, A flexural model for the Paradox Basin: implications for the tectonics of the Ancestral Rocky Mountains: Basin Research, v. 15, p. 97–115, https://doi.org/10.1046/j.1365-2117.2003.00194.x.

Beaumont, C., 1981, Foreland basins: Geophysical Journal International, v. 65, p. 291–329, https://doi.org/10.1111/j.1365-246X.1981.tb02715.x.

Black, B.A., 1975, Geology and oil and gas potential of the northeast Otero platform area, New Mexico: New Mexico Geological Society, Guidebook 26, p. 323–333, https://doi.org/10.56577/FFC-26.323.

Blackwell, D., Richards, M., Frone, Z., Batir, J., Ruzo, A., Dingwall, R., and Williams, M., 2011, Temperature at depth maps for the conterminous U.S. and geothermal resource estimates: GRC Transactions, v. 35, GRC1029452.

Bond, G.C., Nickeson, P.A., and Kominz, M.A., 1984, Breakup of a supercontinent between 625 Ma and 555 Ma: new evidence and implications for continental histories: Earth and Planetary Science Letters, v. 70, no. 2, p. 325–345, https://doi.org/10.1016/0012-821X(84)90017-7.

Chapman, J.B., and McCarthy, R.S., 2013, Detachment levels in the Marathon fold and thrust belt, west Texas: Journal of Structural Geology, v. 49, p. 23–34, http://dx.doi.org/10.1016/j.jsg.2013.01.007.

Dickinson, W.R., and Lawton, T.F., 2003, Sequential intercontinental suturing as the ultimate control for Pennsylvanian Ancestral Rocky Mountains deformation: Geology, v. 31, p. 609–612, https://doi: 10.1130/0091-7613(2003)031<0609: SISATU>2.0.CO;2.

Dickinson, W.R., Klute, M.A., Hayes, M.J., Janecke, S.U., Lundin, E.R., McKittrick, M.A., and Olivares, M.D., 1988, Paleogeographic and paleotectonic setting of Laramide sedimentary basins in the central Rocky –Mountain region: Geological Society of America Bulletin, v. 100, no. 7, p. 1023–1039, https://doi.org/10.1130/0016-7606(1988)100<1023:PAPSOL>2.3.CO;2.

Dutton, S.P., Kim, E.M., Broadhead, R.F., Breton, C.L., Raatz, W.D., Ruppel, S.C., and Kerans, C., 2004, Play analysis and digital portfolio of major oil reservoirs in the Permian Basin: Application and transfer of advanced geological and engineering technologies for incremental production opportunities: University of Texas, Technical Report, https://doi.org/10.2172/828411.

Eichler, C., and Rudolph, K., 2023, Late Paleozoic tectono-stratigraphy of the Mid-Continent: insights from subsidence analysis [abs.]: GSA South-Central Section Annual Meeting.

Ewing, T.E., 1993, Erosional margins and patterns of subsidence in the late Paleozoic west Texas Basin and adjoining basins of west Texas and New Mexico: New Mexico Geological Society, Guidebook 44, p. 155–166, https://doi.org/10.56577/FFC-44.155.

Ewing, T.E., 2019, Tectonics of the west Texas (Permian Basin)—Origins, structural geology, subsidence, and later modification, *in* Ruppel, S.C., ed., Anatomy of the Paleozoic basin: The Permian Basin, USA (vol. 1, ch. 3): The University of Texas at Austin, Bureau of Economic Geology, Report of Investigations 285, AAPG Memoir 118, p. 63–96.

Ewing, T.E., and Christensen, H.V., 2016, Texas through time: Lone Star geology, landscapes, and resources: Bureau of Economic Geology Udden Series, no. 6, p. 1–431, https://doi.org/10.1130/abs/2016SC-273889.

Fairhurst, B., Hanson, M.L., Reid, F., and Pieracacos, N., 2012, WolfBone Play evolution, southern Delaware Basin: Geologic concept modifications that have enhanced economic success: AAPG Search and Discovery Article #10412.

Garner, D.L., and Turcotte, D.L., 1984, The thermal and mechanical evolution of the Anadarko Basin: Tectonophysics, v. 107, no. 1-2, p. 1–24, https://doi.org/10.1016/0040-1951(84)90026-X.

Gradstein, F.G., Ogg, J.G., Schmitz, M.D., and Ogg, G.M., eds., 2020, Geologic time scale 2020: Elsevier, 240 p., https://doi.org/10.1016/C2020-1-02369-3.

Hamlin, H.S., 2009, Ozona sandstone, Val Verde Basin, Texas: Synorogenic stratigraphy and depositional history in a Permian foredeep basin: The American Association of Petroleum Geologists Bulletin, v. 93, no. 5, p. 573–594, https://doi:10.1306/01200908121.

Hantschel, T., and Kauerauf, A.I., 2009, Fundamentals of basin and petroleum systems modeling: Berlin, Springer Science and Business Media, 476 p., https://doi:10.1007/978-3-540-72318-9.

Hickman, R.G., Varga, R.J., and Altany, R.M., 2009, Structural style evolution of the Marathon thrust belt, west Texas: Journal of Structural Geology, v. 31, p. 900–909, doi:10.1016/j.jsg.2008.02.016.

Ingersoll, R.V., Graham, S.A., and Dickinson, W.R., 1995, Remnant ocean basins, *in* Busby, C.J., and Ingersoll, R.V., eds., Tectonics of sedimentary basins: Cambridge, Blackwell, p. 363–391.

Kerans, C., and Kempter, K., 2002, Hierarchical stratigraphic analysis of a carbonate platform, Permian of the Guadalupe Mountains: AAPG Discovery Series, v. 5, CD.

King, W.E., and Harder, V.M., 1985, Oil and gas potential of the Tularosa Basin-Otero platform-Salt Basin graben area, New Mexico: New Mexico Bureau of Mines and Mineral Resources, Circular 198, 36 p., 5 plates.

Kluth, C.F., 1998, Late Paleozoic Deformation of Interior North America: The Greater Ancestral Rocky Mountains: Discussion: AAPG Bulletin, v. 82, no. 12, p. 2272–2227.

Kluth, C.F., and Coney, P.J., 1981, Plate-tectonics of the Ancestral Rocky Mountains: Geology, v. 9, no. 1, p. 10–15, https://doi.org/10.1130/0091-7613(1981)9<10:PTOTAR>2.0.CO;2.

Leary, R.J., Umhoefer, P., Smith, M.E., and Riggs, N., 2017, A three-sided orogen: A new tectonic model for Ancestral Rocky Mountain uplift and basin development: Geology, v. 45, no. 8, p. 735–738, https://doi.org/10.1130/abs/2016AM-280369.

Liu, S., Nummedal, D., and Gurnis, M., 2014, Dynamic versus flexural controls of Late Cretaceous Western Interior Basin, USA: Earth and Planetary Science Letters, v. 389, p. 221–229, https://doi.org/10.1016/j.epsl.2014.01.006.

Loucks, R.G., and Kerans, C., 2019, Geologic review of the Lower Ordovician Ellenburger Group of the Permian Basin, west Texas and southeast New Mexico, *in* Ruppel, S.C., ed., Anatomy of the Paleozoic basin: The Permian Basin, USA (vol. 1, ch. 10): The University of Texas at Austin, Bureau of Economic Geology Report of Investigations 285, AAPG Memoir 118, p. 295–330.

Matchus, E.J., and Jones, T.S., 1984, East-west cross section through Permian Basin of west Texas: west Texas Geological Society Publication.

McBride, E.F., 1978, Olistostrome in the Tesnus Formation (Mississippian-Pennsylvanian), Payne Hills, Marathon region, Texas: Geological Society of America Bulletin, v. 89, p. 1550–1558, https://doi.org/10.1130/0016-7606(1978)89<1550:OITTFM>2.0.CO;2.

Meyer, R.F., 1966, Geology of Pennsylvanian and Wolfcampian Rocks in Southeast New Mexico: New Mexico Bureau of Mines and Mineral Resources, Memoir 17, 123 p., 4 plates, 2 tables, https://doi.org/10.58799/M-17.

Pawlewicz, M., Barker, C.E., and McDonald, S., 2005, Vitrinite reflectance data for the Permian Basin, west Texas and Southeast New Mexico: USGS Open-File Report, 2005-1171, https://doi.org/10.3133/ofr20051171.

Price, B.J., Janson, X., and Kerans, C., 2022, Controls on mixed carbonate-siliciclastic slope morphology, early Permian, northern Delaware Basin, U.S.A.: Marine and Petroleum Geology, v. 143, p. 1–21, https://doi.org/10.1016/j.marpetgeo.2022.105773.

Rudolph, K.W., 2021, The Assembly of Pangea, a view from Laurentia—Paleozoic Orogenies and their Impact on Basin Evolution and Petroleum Systems [abs.]: Dec. 6, 2021, Houston Geological Society Meeting.

Ruppel, S.C., ed., 2019, Anatomy of the Paleozoic basin: The Permian Basin, USA (vol. 1): The University of Texas at Austin, Bureau of Economic Geology Report of Investigations 285, AAPG Memoir 118, 412 p., https://doi.org/10.23867/RI0285-1.

Saylor, J.E., Jordan, J.C., Sundell, K.E., Wang, X., Wang, S., and Deng, T., 2017, Topographic growth of the Jishi Shan and its impact on basin and hydrology evolution, NE Tibetan Plateau: Basin Research, v. 30, no. 3, p. 544–563, https://doi.org/10.1111/bre.12264.

Silver, B.A., and Todd, R.G., 1969, Permian cyclic strata, northern Midland and Delaware Basins, west Texas and southeastern New Mexico: The American Association of Petroleum Geologists, Bulletin 53, p. 2223–2251, https://doi.org/10.1306/5D25C94D-16C1-11D7-8645000102C1865D.

Soreghan, G.S., Keller, G.R., Gilbert, M.C., Chase, C.G., and Sweet, D.E., 2012, Load-induced subsidence of the Ancestral Rocky Mountains recorded by preservation of Permian landscapes: Geosphere, v. 8, no. 3, p. 654–668.

Spangler, L.R., 2021, Timing and controls on Late Paleozoic tectonism and synorogenic sedimentation, Bursum Formation, Sacramento Mountains, New Mexico, USA [M.S. thesis]: Austin, University of Texas, 76 p.

Sweet, D.E., Brotherton, J.L., Chowdhury, N.U.M.K., and Ramsey, C.E., 2021, Tectonic subsidence analysis of the Ancestral Rocky Mountains from the interior to the southern margin: Palaeogeography, Palaeoclimatology, Palaeoecology, v. 576, p. 1–16, https://doi.org/10.1016/j.palaeo.2021.110508.

Tesauro, M., Kaban, M.K., and Mooney, W.D., 2015, Variations of the lithospheric strength and elastic thickness in North America: Geochemistry, Geophysics, Geosystems, v. 16, p. 2197–2220, https://doi.org/10.1002/2015GC005937.

Tufano, B.C., and Pietras, J.T., 2017, Coupled flexural-dynamic subsidence modeling approach for retroforeland basins: Example from the Western Canada Sedimentary Basin: GSA Bulletin, v. 129, no. 11/12, p. 1622–1635, https://doi.org/10.1130/B31646.1.

Wangen, M., 2010, Physical principles of sedimentary basin analysis: Cambridge, Cambridge University Press, p. 527, https://doi.org/10.1017/CBO9780511711824.

Ye, H., Royden, L., Burchfiel, C., and Schuepbach, M., 1996, Late Paleozoic Deformation of Interior North America: The Greater Ancestral Rocky Mountains: The American Association of Petroleum Geologists, Bulletin 80, no. 9, p. 1397–1432, https://doi.org/10.1306/64ED9A4C-1724-11D7-8645000102C1865D.

Yonkee, W.A., and Weil, A.B., 2015, Tectonic evolution of the Sevier and Laramide belts within the North American Cordillera orogenic system: Earth-Science Reviews, v. 150, p. 531–593, https://doi.org/10.1016/j.earscirev.2015.08.001.

Zhang, H., Mann, P., Bird, D.E., and Rudolph, K., 2021, Integration of regional gravity modeling, subsidence analysis, and source rock maturity data to understand the tectonic and hydrocarbon evolution of the Permian Basin, west Texas: Interpretation, v. 9, no. 1, https://doi.org/10.1190/INT-2020-0065.1.

Appendices can be found at
https://nmgs.nmt.edu/repository/index.cfml?rid=2023001